Investigation of mechanical stability of possible structures of PtN using first-principles computations

S. K. R. Patil,[1] S. V. Khare,[2*] B. R. Tuttle,[3] J. K. Bording,[4] and S. Kodambaka[5]

[1]*Department of Mechanical Engineering, The University of Toledo, Toledo, Ohio, USA.*

[2]*Department of Physics and Astronomy, The University of Toledo, Toledo, Ohio, USA.*

[3]*School of Science , Behrend College, Penn State University at Erie, PA, 16513.*

[4]*Center for Functional Nanomaterials, Brookhaven National Lab, Upton, NY 11973, USA.*

[5]*IBM Research Division, T.J. Watson Research Center, Yorktown Heights, New York 10598, USA*

ABSTRACT

We report an *ab initio* study of the mechanical stability of platinum nitride (PtN), in four different crystal structures, the rock salt (rs-PtN), zinc blende (zb-PtN), cooperite and a face centered orthorhombic phase. Only the rs-PtN phase is found to be stable and has the highest bulk modulus B = 284 GPa. Its electronic density of states shows no band gap making it metallic. The zb-PtN phase does not stabilize or harden by the nitrogen vacancies investigated in this study. Therefore, the experimental observation of super hardness in PtN remains a puzzle.

I. INTRODUCTION

Metal and semi-conductor nitrides are an important class of materials having properties of fundamental interest as well as those used in a variety of applications.[1,2,3,4]

* Corresponding author email: khare@physics.utoledo.edu

Despite the wide interest in making ever better nitrides for applications, the noble metal nitrides have evaded discovery till recently. Despite the wide interest in metal nitrides, noble metal nitrides have evaded discovery until the recent synthesis of gold [5] and platinum nitrides. In 2004 Gregoryanz *et al*.[6] reported the synthesis of platinum nitride, PtN. This compound was formed using laser-heated diamond anvil-cell techniques at pressures greater than 45 GPa and temperatures exceeding 2000 K. The compound was then recovered completely at room temperature and pressure and analyzed by electron microprobe techniques. Compositional profiles showed that the Pt to N ratio was close to 1:1 with a little variation given by the formula PtN_{1-x} where $x < 0.05$. The synchrotron x-ray diffraction experiment revealed PtN to be face-centered cubic but was unable to distinguish between zinc-blende (zb-PtN) and rocksalt (rs-PtN) structures due to a much stronger Pt signal caused by the large difference between masses of Pt and N. But PtN had a first – order Raman spectrum and hence rocksalt structure was ruled out.[6] As the two first order bands obtained[6] seemed to correspond to Raman active peaks of a zinc-blende structure, the PtN synthesized was concluded to be of this form. The bulk modulus (B) of this zinc-blende PtN was determined to be 372 ± 5 GPa. This B is comparable to 382 GPa of super hard cubic zinc-blende structure BN[7]. Thus PtN with a zinc-blende structure is the first noble metal nitride experimentally identified to be a super hard material. However, theoretical calculations fail to confirm the high bulk modulus extracted from experiment.

Recent theoretical investigations have applied different density functional methods to calculate the lattice constants and bulk moduli of various forms of PtN. These studies conclude that the lattice constant of the zb-PtN is consistent with

experiments. However, these calculations draw contradictory conclusions about the high bulk modulus of PtN found in experiment. The bulk modulus reported in Ref. [8] concurs with the experimental value but the value reported by Ref. [9] contradicts both the experiment and Ref. [8], since it is smaller by a factor of one half. Another investigation, in Ref. [10] gives a variety of different values for B depending on the method used.

These explorations motivated us to study theoretically different crystal structures of PtN as possible candidates for super-hardness. We restricted our study to compounds with 1:1 stoichiometric ratio of Pt:N (except for PtN_2, cf. section VIII). Two of these, the zb- and rs- PtN phases were motivated by results of X ray measurements[6]. The zb-PtN was found to be mechanically unstable and transformed to a lower energy fco-PtN phase for strain type 1 given in Table I. Thus fco-PtN was studied as a potential phase for super hard PtN. PtS exists in cooperite phase and hence cooperite PtN (co-PtN) was also studied as a possible phase for super hard PtN. The main results of our investigations are as follows. The zb-PtN was found to have a lattice constant close to experiment; however, it was also found to be mechanically unstable and transformed to a lower energy fco-PtN. The bulk modulus of zb-PtN was found from two different methods to be almost half the experimentally derived value consistent with the value reported in Ref. [9]. Our bulk modulus results are therefore consistent with Ref. [9]. The higher values reported in Refs. [8] and [10] are higher by a factor of two due to errors in calculation. Only the rs-PtN phase was found to be mechanically stable i.e. its elastic constants obey the conditions $(C_{11} - C_{12}) > 0$, $(C_{11} + 2C_{12}) > 0$, $C_{11} > 0$, and $C_{44} > 0$. It has the highest bulk modulus (B = 284 GPa) greater than the value of 230 GPa for the zb-PtN phase. This lower value of B in the zb-PtN phase (compared to the experimental value of 372 GPa[6])

and also its instability led us to investigate the effect of N vacancies on these properties. We found that for nitrogen vacancy concentrations of 3.7% and 12.5% that bracketed the value of the maximum 5% reported in experiment, the zb-PtN phase remained unstable and its B hardly changed. Our study indicates that further experimental investigation needs to be carried out to find the cause of the stability and high B of the zb-PtN.

The rest of the paper is organized as follows. Section II gives the details of the *ab initio* method used. Section III describes the structure of four different phases of PtN studied. Section IV illustrates the method of calculation of elastic constants. In section V we investigate the stability of the four phases. Section VI reports the band structure and density of states of rs-PtN. Section VII gives results involving introduction of N vacancies. Section VIII gives the results and discussion on bulk modulus calculated for different phases of PtN studied.

II *AB INITIO* METHOD

We performed first-principles total energy calculations within the local density approximation (LDA) and also generalized gradient approximation (GGA) to the density functional theory[11] (DFT) using the suit of codes VASP.[12,13,14,15] Core electrons are implicitly treated by ultra soft Vanderbilt type pseudopotentials[16] as supplied by G. Kresse and J. Hafner[17]. For each calculation, irreducible *k*-points are generated according to the Monkhorst-Pack scheme.[18] Convergence is achieved with 408 *k*- points in the irreducible part of Brillouin zone for zb-PtN and rs-PtN structures and with 512 and 864 *k*- points for cooperite and orthorhombic structures respectively. The single-particle wave functions have been expanded in a plane-wave basis using a 224 eV kinetic energy cutoff.

All atoms are allowed to relax until a force tolerance of 0.03 eV/Å is reached for each atom. Tests using a higher plane-wave cutoff and a larger k-point sampling indicate that a numerical convergence better than ±1.0 meV is achieved for relative energies.

III. CRYSTAL STRUCTURE

We investigated four different phases of PtN, the (i) zb-PtN structure (space group $F\bar{4}3m$)[19], (ii) rs-PtN structure (space group $Fm\bar{3}m$)[19], (iii) face-centered orthorhombic structure (fco) (space group $Fddd$)[19] and (iv) cooperite (PtS) structure (space group $P4_2/mmc$)[19]. The unit cells for the first three phases are shown Figs. 1, 2, and 3 respectively. They consist of three lattice constants of the conventional unit cell a, b, and c with lattice vectors $\mathbf{a}_1 = \frac{1}{2}$(0, b, c), $\mathbf{a}_2 = \frac{1}{2}$ (a, 0, c) and $\mathbf{a}_3 = \frac{1}{2}$ (a, b, 0). The basis consists of a Pt atom at (0, 0, 0) and an N atom at $\frac{1}{\alpha}(\mathbf{a}_1 + \mathbf{a}_2 + \mathbf{a}_3)$. The first two phases have c = b = a, giving them a cubic symmetry. The first phase has α = 4, while the second and third phases have α = 2. Fig. 4. shows the unit cell of co-PtN having lattice constants a and c. The lattice vectors are $\mathbf{a}_1$ = (a, 0, 0), $\mathbf{a}_2$ = (0, a, 0) and $\mathbf{a}_3$ = (0, 0, c). Two Pt atoms at (0, 0, 0), $\frac{1}{2}(\mathbf{a}_1 + \mathbf{a}_2 + \mathbf{a}_3)$ and two N atoms at $\left(\frac{1}{2}\mathbf{a}_2 + \frac{1}{4}\mathbf{a}_3\right)$, $\left(\frac{1}{2}\mathbf{a}_2 + \frac{3}{4}\mathbf{a}_3\right)$ make up the basis.

The equilibrium lattice constants a, b, and c were varied independently (when they were different) to obtain the absolute minimum in total energy for each structure. All basis atoms were allowed to relax fully. Table V summarizes the equilibrium lattice

constants of the different PtN structures. The structure with the lowest total energy per formula unit of PtN was co-PtN. Hence the **f**ormation energies, E_{f-r-t}, of the other phases are reported with **r**espect to **t**etragonal structure in Table V.

IV. ELASTIC CONSTANTS

Elastic constants are the measure of the resistance of a crystal to an externally applied stress. For small strains Hooke's law is valid and the crystal energy E is a quadratic function of strain.[20] Thus, to obtain the total minimum energy for calculating the elastic constants to second order, a crystal is strained and all the internal parameters relaxed. Consider a symmetric 3×3 strain tensor $\boldsymbol{\varepsilon}$ which has matrix elements ε_{ij} (i, j = 1, 2, and 3) defined by Eq. (1)

$$\varepsilon_{ij} \equiv I_{ij}\, e_i + \frac{1}{2}\left(1 - I_{ij}\right) e_{9-i-j}. \qquad (1)$$

Such a strain transforms the three lattice vectors defining the unstrained Bravais lattice $\{\mathbf{a}_k$, k = 1, 2, and 3$\}$ to the strained vectors[21] $\{\mathbf{a}'_k$, k = 1, 2, and 3$\}$ as given by Eq. (2)

$$\mathbf{a}'_\mathbf{k} = \left(\mathbf{I} + \boldsymbol{\varepsilon}\right).\, \mathbf{a}_\mathbf{k}, \qquad (2)$$

where **I** is defined by its elements, $I_{ij} = 1$ for $i = j$ and 0 for $i \neq j$. Each lattice vector $\mathbf{a}_k$ or $\mathbf{a}'_k$ is a 3×1 matrix. The change in total energy due to above strain (1) is

$$\frac{\Delta E}{V_0} \equiv \frac{E\left(\{e_i\}\right) - E_0}{V_0} = \left(1 - \frac{V}{V_0}\right) P\left(V_0\right) + \frac{1}{2}\left(\sum_{i=1}^{6}\sum_{j=1}^{6} C_{ij} e_i e_j\right) + O\left(\{e_i^3\}\right), \qquad (3)$$

where V_0 is the volume of the unstrained lattice, E_0 is the total minimum energy at this unstrained volume of the crystal, $P(V_0)$ is the pressure of the unstrained lattice, and V is the new volume of the lattice due to strain in Eq. (1). In Eq. (3), $C_{ij} = C_{ji}$ due to crystal

symmetry.[20] This reduces the elastic stiffness constants C_{ij}, from 36 to 21 independent elastic constants in Eq. (3). Further crystal symmetry[20] reduces the number to 9 (C_{11}, C_{12}, C_{13}, C_{23}, C_{22}, C_{33}, C_{44}, C_{55}, C_{66}) for orthorhombic crystals, 6 (C_{11}, C_{12}, C_{13}, C_{33}, C_{44}, C_{66}) for tetragonal crystals and 3 (C_{11}, C_{12}, C_{44}) for cubic crystals. A proper choice of the set of strains $\{e_i, i=1, 2, ... 6\}$, in Eq. (3) leads to a parabolic relationship between $\Delta E / V_0$ ($\Delta E \equiv E - E_0$) and the chosen strain. Such choices for the set $\{e_i\}$ and the corresponding form for ΔE are shown in Table I[22] for cubic, Table II[23] for tetragonal and Table III[24] for orthorhombic lattices. For each lattice structure of PtN studied, we strained the lattice by 0%, $\pm 1\%$, and $\pm 2\%$ to obtain the total minimum energies E(V) at these strains. These energies and strains were fit with the corresponding parabolic equations of $\Delta E / V_0$ as given in Tables I, II and III to yield the required second order elastic constants. While computing these energies all atoms are allowed to relax with the cell shape and volume fixed by the choice of strains $\{e_i\}$.

V. MECHANICAL STABILITY

The strain energy $\left(\frac{1}{2} C_{ij} e_i e_j\right)$ of a given crystal in Eq. (3) must always be positive for all possible values of the set $\{e_i\}$; otherwise the crystal would be mechanically unstable. This means that the quadratic form $\left(\frac{1}{2} C_{ij} e_i e_j\right)$ must be positive definite for all real values of strains unless all the strains are zero. This imposes further restrictions on the

elastic constants C_{ij} depending on the crystal structure. These stability conditions can be found out by standard algebraic methods.[25]

a. zb-PtN

For cubic crystal structures such as those of zb-PtN or rs-PtN, the necessary conditions for mechanical stability are given by[26]

$$(C_{11} - C_{12}) > 0,\ (C_{11} + 2C_{12}) > 0,\ C_{11} > 0,\ C_{44} > 0. \qquad (4)$$

The elastic constants are determined by applying the strains listed in Table I. $C_{11} - C_{12}$ is obtained by using the strain combination on the first row of Table I. Table IV shows the numerical values of our computation of all the elastic constants of zb-PtN. These values satisfy all the stability conditions of Eq. (4) except the condition that $(C_{11} - C_{12}) > 0$. Thus we have concluded that the zb-PtN is mechanically unstable which contradicts the experimental data.[6]

We now turn our attention to the strain used on the second row of Table I which is an isotropic strain and it yields, $B \equiv \frac{C_{11}+2C_{12}}{3}$.We obtained a B value of 230 GPa, which is lower than the experimentally reported value of 372 GPa by 38%.[6] The fit of these isotropically strained volumes and corresponding total minimum energies to Murnaghan equation of state[27] yielded B = 231 GPa. Thus our theoretical calculations suggest that the experimentally observed structure is unstable and with a B that is far larger than the theoretically expected value. However, the experiment found that the precise stoichiometry for their PtN sample was given by PtN_{1-x} with $0 < x < 0.05$. To investigate the effect of N vacancies on the stability of zb-PtN and value of B, we did

further calculations which are described in section VII. Based on our results we conclude that N vacancies only soften the material and do not explain the large experimental value for B (372 GPa).

These disagreements between our theoretically computed properties and the experimental results for zb-PtN motivated us to explore other possible structures of PtN which could potentially yield very large values of the elastic constants and hence super-hardness. Since Pt has a large value of B = 298 GPa[28] it would seem plausible to have such an expectation.[6] The X-ray diffraction part of the experimental measurements could not distinguish[6, 8] between the zb-PtN and rs-PtN structural types since they both had face centered cubic (fcc) symmetry. This is because of the much weaker signal of N atoms than that of Pt atoms due to a large difference in their atomic numbers. Also many other mono transition metal nitrides, such as CrN, NbN, VN, and ZrN exist in the NaCl phase. So we explored this phase next.

b. rs-PtN

As rs-PtN is cubic, it has to satisfy all the conditions in Eq. (4) to be mechanically stable. These conditions are indeed satisfied as seen from the calculated elastic constants in Table IV, making it mechanically stable. The calculated B with the parabolic fit of strain 2 in Table I was found to be 284 GPa. As zb-PtN is unstable and rs-PtN is stable and because of the fcc structure reported by the X ray analysis[6], one would be tempted to conclude that PtN is a rock salt structure like many other monotransition metal nitrides. But the calculated lattice constant of rock salt PtN, 0.45036 nm (by GGA) and 0.44071 nm (by LDA) varies substantially from 0.4801 nm measured experimentally.[6] The value

of B we obtained was 284 GPa, still off from the experimental value of 372 GPa. It is thus not clear whether the observed PtN is in NaCl structure. We nonetheless, explored the electronic properties of this stable phase which are described in section VI. With an interest toward finding a super-hard form of PtN we explored two other structures of PtN having 1:1 stoichiometry. The first of these, the tetragonal (cooperite) structure was motivated by the existence in this form of PtO which could exist as a contaminant in the experimental sample.[29]

c. *co-PtN*

The stability criteria for a tetragonal crystal[26] are:

$$\left(C_{11}-C_{12}\right)>0,\ \left(C_{11}+C_{33}-2c_{13}\right)>0,\ \left(2C_{11}+C_{33}+2C_{12}+4C_{13}\right)>0,\\ C_{11}>0,\ C_{33}>0,\ C_{44}>0,\ C_{66}>0. \qquad (5)$$

The elastic constants of tetragonal PtN are shown in Table IV. The calculated elastic constant C_{44} is negative violating Eq. (5) and so is labeled unstable in Table IV. For the strain types 1, 2, 4, 5 and 6 in Table II the total minimum energy for strained lattice was less than that of the unstrained lattice indicating the transformation of the tetragonal structure to either monoclinic or triclinic structures. Hence, the elastic constants $C_{11}, C_{12}, C_{13}, C_{66},$ and C_{33} are labeled unstable in Table IV, making the tetragonal cell mechanically unstable. Thus the formation of stable PtN in cooperite phase is ruled out. The fourth structure we investigated was discovered by noticing that $C_{11}-C_{12} < 0$ in Table IV for the zb-PtN. Under the strain corresponding to $C_{11}-C_{12}$ the ZnS structure transforms to a face centered orthorhombic (fco) structure.

d. fco-PtN

The mechanical stability criteria for face centered orthorhombic[24] PtN are:

$$(C_{22}+C_{33}-2C_{23})>0,\ \ (C_{11}+C_{22}+C_{33}+2C_{12}+2C_{13}+2C_{23})>0,$$

$$C_{11}>0,\ C_{22}>0,\ C_{33}>0,\ C_{44}>0, C_{55}>0,\ C_{66}>0. \qquad (6)$$

The calculated elastic constants are shown in Table IV. All the elastic constants obey the mechanical stability criteria given in Eq. (6) except for C_{44}. Hence the possibility of PtN crystallizing in face centered orthorhombic phase is eliminated. For strain type 4 in Table III the fco PtN transforms to a triclinic phase, which we did not investigate. We now conclude that of the four forms of PtN we studied only the rs-PtN is mechanically stable. We describe its electronic structure next.

VI. ELECTRONIC STRUCUTRE OF rs-PtN

The band structure of this phase along a high symmetry direction is shown in Fig. 5. The calculated density of states (DOS) is shown in Figure 6. There is no band gap in the DOS at the fermi level (E_F) and hence rs-PtN is metallic. The bands near the fermi level are mainly contributed by platinum d-orbitals while the lowest band is mainly the nitrogen s-orbital. The electronic density of states is calculated using 408 irreducible *k*-points and a 0.2 eV smearing of the energy levels to provide a smooth DOS plot. The DOS between -5 eV and +1 eV is dominated by the Pt metal states and compares well to the photoemission spectra of platinum[30]. Figure 7. shows the projected density of states (PDOS) of Pt and N atoms in s, p and d orbitals. As seen from PDOS, the d electrons of Pt contribute to the majority of the DOS near the Fermi level.

VII. NITROGEN VACANCIES

The experimental specimen of PtN_{1-x} was sub-stoichiometric with $0 < x < 0.05$. This sub-stoichiometry may be the reason for both its stability and high value of B. To check for such a trend, we performed a calculation with a larger supercell[31] to create $Pt_{27}N_{26}$ (i.e. x = 0.0370) which is comparable to the experimental specimen. The equilibrium lattice constant for this sub stoichiometric zb-PtN was found to be 0.46019 nm and B was found to be 221 GPa. Thus the bulk modulus is reduced slightly at this nitrogen vacancy concentration. The other sub-stoichiometry computed was a supercell[32] of Pt_8N_7 (i.e. x = 0.125). The lattice constant and bulk modulus for this compound were 0.45556 nm and 238 GPa respectively. Thus this composition hardly raises the value of B to the value reported in experiment. The strain type 1 of Table I for which the zb-PtN was unstable was applied to the above mentioned two super cells. These calculations showed that the stability criterion $(C_{11} - C_{12}) > 0$ was not satisfied for these sub-stoichiometric forms either. Values of x in our calculations for sub-stoichiometric cases range from 0 (no vacancies), 0.037 and 0.125. These values cover the experimental range for x from 0 to 0.05 and beyond. It seems unlikely then that PtN_{1-x} ($0 < x < 0.05$), can be stabilized by the presence of vacancies alone. However, stabilizing and hardening effects due to other types of defects or impurities induced by the high pressure and high temperature production technique used in the experiment cannot be ruled out.

VIII. BULK MODULUS RESULTS AND DISCUSSION

Table V lists our values of B for zb-PtN and rs-PtN calculated using VASP with LDA and also the generalized gradient approximation, GGA. As a test of our method we also

calculated the bulk modulus of zinc blende structure of BN and rock salt OsN with LDA. Our B = 382 GPa for BN is in very good agreement with the experimental value of 382 GPa[7] and previous LDA value of 403 GPa.[33] Also our calculated bulk modulus value of 380 GPa for OsN is in good agreement with 372 GPa obtained by a previous *ab initio* calculation.[34] However, our results using VASP with GGA for PtN differ significantly from those of Ref. [8][38] as seen in Table V. Our value of B = 192 GPa with GGA for zb-PtN is about 48% smaller than their value of 371 GPa which is almost identical to the experimental value[6]. However, our value matches quite well with the value of 194 GPa found in Ref. [9]. Note that an all electron method WIEN2K[35] was used in both Refs. [8] and [9], while our VASP method is based on pseudo-potentials. For a proper comparison we also computed these bulk moduli with WIEN2K. We used FLAPW calculations with LDA and GGA as done in Refs. [8] and [9] using WIEN2K. Non over lapping muffin-tin sphere radii of 0.0100 nm and 0.0085 nm were used for Pt and N atoms respectively. Using this method we obtained B = 178 GPa for zb-PtN as seen in Table V, which is in good agreement with our value of 192 GPa obtained using VASP. A similar situation arises for rs-PtN with GGA where our WIEN2K result is B = 233 GPa in agreement with VASP value of 226 GPa but different from 431 GPa of Ref. [8][38]. The LDA and GGA bulk moduli for zb-PtN obtained in Ref. [9], which also uses WIEN2K are given in Table V. They are in good agreement with our present work. For zb-PtN, the shear modulus, $C' = \frac{C_{11} - C_{12}}{2}$ = -17 GPa obtained in Ref. [9] is in good agreement with -15.5 GPa obtained by us.

R. Yu et al.[9], have suggested that the experimental sample may contain excess N atoms, and hence may well be the PtN_2 flourite phase in the $Fm\bar{3}m$ space group. As a

check, we also calculated the bulk modulus and elastic constants of PtN_2 using VASP. The bulk modulus was found to be 300 GPa. The computed elastic constants C_{11}, C_{12} and C_{44} were 495 GPa, 193 GPa and 109 GPa respectively, satisfying the mechanical stability conditions for cubic lattices as given in Eq. (4). These values for fluorite PtN_2 are in good agreement with those obtained in Ref. [9]. It is interesting to note that though the value for B clearly disagrees with the experimental value it is the only phase for which C_{44} is of extremely high value 495 GPa comparable to that of super hard BN[36]. It is also interesting to note that values for B in Ref. [8][38] are approximately $\frac{1}{2}$ of our values using WIEN2K and those of Ref. [9].

SUMMARY

Using first principles calculations we have computed properties of PtN, a recently synthesized noble metal nitride[6]. Using our *ab initio* calculations the experimental zinc-blende structure of PtN reported[6] was found to be mechanically unstable and its bulk modulus was found to be 38% lower than in experiment. Upon introduction of N vacancies in this zb-PtN structure we found that it remained unstable and the bulk modulus did not change substantially. The role of other types of impurities or defects causing the stability and super-hardness cannot be ruled out. Further experimental investigation is needed to understand the underlying causes behind the stability and super-hardness, which are not explained by our *ab initio* calculations.

To find super-hardness in other forms of PtN we also investigated its rock-salt, cooperite, and face centered orthorhombic phases. Of these only rs-PtN was found to be stable. X-ray diffraction measurements[6] have identified this form as a possible structural candidate showing fcc symmetry. However, our calculated lattice constant 0.45036 nm differs from the experimental value of 0.48010 nm by 6.2%. We also find no evidence for super-hardness in this form. The electronic band structure and total density of states of this stable form were studied. This form shows no band gap and is metallic consistent with experimental observation. All our computations and those of others[8,9,10] reveal that more experiments need to be performed to ascertain the true nature of the newly discovered PtN material.

This work was partially supported by the Division of Materials Sciences, Office of Basic Energy Science, US Department of Energy. S. V. Khare acknowledges support from the

University of Toledo, Office of Research, URAF 2005 award. We thank Ohio Supercomputer Center for providing computing resources.

REFERENCES

[1] M. W. Barsoum, Prog. Sol. St. Chem. **28**, 201 (2000).

[2] J. S. Chun, I. Petrov, and J. E. Greene, J. Appl. Phys. **86**, 3633 (1999).

[3] A. E. Kaloyeros and E. Eisenbraun, Annu. Rev. Mater. Sci. **30**, 363 (2000).

[4] S. H. Jhi, J. Ihm, S. G. Louie, and M. L. Cohen, Nature **399**, 132 (1999).

[5] S. Krishnamurthy, M. Montalti, M. G. Wardle, M. J. Shaw, P. R. Briddon, K. Svensson, M. R. C. Hunt, and L. Siller, Phys. Rev. B **69**, 1 (2004).

[6] E. Gregoryanz, C. Sanloup, M. Somayazulu, J. Bardo, G. Fiquet, H-. K. Mao, and R. Hemley, Nat. Mater. **3**, 294 (2004).

[7] E. V. Yakovenko, I. V. Aleksandrov, A. F. Gonchavrov, and S. M. Stishov, Sov. Phys. JETP **68**, 1213 (1989).

[8] B. R. Sahu and L. Kleinman, Phys. Rev. B **71**, 041101 (R) (2005).

[9] R. Yu and X. F. Zhang, Appl. Phys. Lett. **86**, 121913 (2005)

[10] Uddin, Jamal, Scuseria, and E. Gustavo, Phys. Rev. **B** 72, 035101 (2005).

[11] P. Hohenberg and W. Kohn, Phys. Rev. **136**, B864 (1964); W. Kohn and L. J. Sham, Phys. Rev. **140**, A1133 (1965).

[12] G. Kresse and J. Hafner, Phys. Rev. **B** 47, RC558 (1993).

[13] G. Kresse, Thesis, Technische Universiät Wien 1993.

[14] G. Kresse and J. Furthmüller, Comput. Mat. Sci. **6**, 15 (1996).

[15] G. Kresse and J. Furthmüller, Phys. Rev. B **54,** 11169 (1996).

[16] D.Vanderbilt, Phys. Rev. B **41** 7892 (1990).

[17] G. Kresse and J. Hafner, J. Phys.: Condens. Matter **6**, 8245 (1994).

[18] H. J. Monkhorst and J. D. Pack, Phys. Rev. B **13**, 5188 (1976).

[19] See for different crystal models: http://cst-www.nrl.navy.mil/lattice/prototype.html.

[20] J. F. Nye, *Physical properties of crystals, Their representation by tensors and matrices*, (Oxford press, 1957), Chap VIII.

[21] *Intermetallic compounds : Principles and Practice, Vol I: Principles*, J. H. Westbrook and R. L. Fleischer, eds., John Wiley and Sons (London, 1995), ch. 9 (Pg 195-210).

[22] M. J. Mehl, J. E. Osburn, D. A. Papaconstantopoulos, and B. M. Klein, Phys. Rev. B **41**, 10311 (1990); *ibid* **42**, 5362(E) (1990).

[23] M. Alouani, R. C. Albers, and M. Methfessel, Phys. Rev. B **43**, 6500 (1991).

[24] O. Beckstein, J. E. Klepeis, G. L. W. Hart, and O. Pankrtov, Phys. Rev. B **63**, 134112 (2001).

[25] W.L. Ferrar, *Algebra; a text-book of determinants, matrices, and algebraic forms*, (1941) (Pg. 138).

[26] D. C. Wallace, *Thermodynamics of Crystals* (Wiley, New York, 1972), Chap. 1.

[27] F. D. Murnaghan, Proc. Natl. Acad. Sci. U.S.A. **30**, 244 (1944).

[28] J. J. Gilman, *Electronic Basis of the Strength of Materials*, (Cambridge University Press,UK, 2003), Chap. 12.

[29] As an example: It is known that TiO is iso-structural with NaCl structure of TiN and that both have similar lattice constants. See : S. Kodambaka, S. V. Khare, V. Petrova, D. D. Johnson, I. Petrov, and J. E. Greene, Phys. Rev. B **67**, 35409 (2003).

[30] S. F. Lin, D. T. Pierce, and W. E. Spicer, Phys. Rev. B **4**, 326 (1971).

[31] A $3\times3\times3$ array of unit cells with 2 atoms per unit cell in fcc symmetry (1 Pt and 1 N), results in 54 atoms (27 Pt and 27 N atoms). We removed 1 N atom to get $Pt_{27}N_{26}$.

[32] A $2\times2\times2$ array of unit cells with 2 atoms per unit cell in fcc (1 Pt and 1 N), results in 16 atoms (8 Pt and 8 N atoms). We removed 1 N atom to get Pt_8N_7.

[33] K. Shimada, T. Sota, and K. Suzuki, J. Appl. Phys., 84, 4951 (1998).

[34] J. C. Grossman, A. Mizel, M. Cote, M. L. Cohen, and Steven G. Louie, Phys. Rev. B **60**, 6343 (1999).

[35] P. Blaha, K. Schwarz, G. K. H. Madsen, D. Kvasnicka, and J. Luitz, WIEN2K (Vienna University of Technology, Vienna, Australia, 2001).

[36] M. Grimsditch, E. S. Zouboulis, and A. Polian, J. Appl. Phys., 76, 832 (1994)

[37] The high symmetry *k*- point X (0, 1, 0) is identical by symmetry to (1, 1, 0); cf. http://cst-www.nrl.navy.mil/bind/static/example7/index.html

[38] Just before submission we received a private communication from Prof. L. Kleinman that the values of B in Ref. [8] have been overestimated by a factor of 2 thus agreeing with our results and those of Ref. [9].

TABLES

Strain	Parameters (unlisted $e_i = 0$)	$\Delta E / V_0$
1	$e_1 = e_2 = \delta$, $e_3 = (1+\delta)^{-2} - 1$	$3(C_{11} - C_{12})\delta^2$
2	$e_1 = e_2 = e_3 = \delta$	$\frac{3}{2}(C_{11}+2C_{12})\delta^2$
3	$e_6 = \delta, e_3 = \delta^2 (4-\delta^2)^{-1}$	$\frac{1}{2} C_{44} \delta^2$

TABLE I. Three strain combinations in the strain tensor [Eq. (1)] for calculating the three elastic constants of cubic structures shown in Fig. 1 and Fig. 2. The three independent elastic constants C_{11}, C_{12}, and C_{44} of zinc blende and rock salt PtN are calculated from the above strains. Symmetry dictates $C_{ij} = C_{ji}$ and all unlisted $C_{ij} = 0$. The strain δ is varied in steps of 0.01 from δ = -0.02 to 0.02. ΔE [Eq. (3)] is the difference in energy between that of the strained lattice and the unstrained lattice. The equilibrium or unstrained lattice volume is V_0.

Strain	Parameters (unlisted $e_i = 0$)	$\Delta E / V_0$
1	$e_1 = \delta$	$\frac{1}{2} C_{11} \delta^2$
2	$e_3 = \delta$	$\frac{1}{2} C_{33} \delta^2$
3	$e_4 = 2\delta$	$2 C_{44} \delta^2$
4	$e_1 = 2\delta, e_2 = e_3 = -\delta$	$\frac{1}{2}(5C_{11} - 4C_{12} - 2C_{13} + C_{33})\delta^2$
5	$e_1 = e_2 = -\delta, e_3 = 2\delta$	$(C_{11} + C_{12} - 4C_{13} + 2C_{33})\delta^2$
6	$e_1 = e_2 = \delta, e_3 = -2\delta, e_6 = 2\delta$	$(C_{11} + C_{12} - 4C_{13} + 2C_{33} + 2C_{66})\delta^2$

TABLE II. Six strain combinations in the strain tensor [Eq. (1)] for calculating the six elastic constants of the tetragonal structure shown in Fig. 3. The six independent elastic constants C_{11}, C_{12}, C_{13}, C_{33}, C_{44}, and C_{66} of tetragonal PtN are calculated from the above strains. Symmetry dictates $C_{ij} = C_{ji}$ and all unlisted $C_{ij} = 0$. The strain δ is varied in steps of 0.01 from δ = -0.02 to 0.02. ΔE [Eq. (3)] is the difference in energy between that of the strained lattice and the unstrained lattice. The equilibrium or unstrained lattice volume is V_0.

Strain	Parameters (unlisted $e_i = 0$)	$\Delta E / V_0$
1	$e_1 = \delta$	$\frac{1}{2} C_{11} \delta^2$
2	$e_2 = \delta$	$\frac{1}{2} C_{22} \delta^2$
3	$e_3 = \delta$	$\frac{1}{2} C_{33} \delta^2$
4	$e_4 = \delta$	$\frac{1}{2} C_{44} \delta^2$
5	$e_5 = \delta$	$\frac{1}{2} C_{55} \delta^2$
6	$e_6 = \delta$	$\frac{1}{2} C_{66} \delta^2$
7	$e_1 = 2\delta, e_2 = e_3 = -\delta$	$\frac{1}{2}(4C_{11} - 4C_{12} - 4C_{13} + C_{22} + 2C_{23} + C_{33})\delta^2$
8	$e_1 = -\delta, e_2 = 2\delta, e_3 = -\delta$	$\frac{1}{2}(C_{11} - 4C_{12} + 2C_{13} + 4C_{22} - 4C_{23} + C_{33})\delta^2$
9	$e_1 = e_2 = -\delta, e_3 = 2\delta$	$\frac{1}{2}(C_{11} + 2C_{12} - 4C_{13} + C_{22} - 4C_{23} + 4C_{33})\delta^2$

TABLE III. Nine strain combinations in the strain tensor [Eq. (1)] for calculating the nine elastic constants of the orthorhombic structure shown in Fig. 4. The nine independent elastic constants C_{11}, C_{12}, C_{13}, C_{23}, C_{22}, C_{33}, C_{44}, C_{55}, and C_{66} of the orthorhombic PtN are calculated form the above strains. Symmetry dictates $C_{ij} = C_{ji}$ and all unlisted $C_{ij} = 0$. The strain δ is varied in steps of 0.01 from δ = -0.02 to 0.02. ΔE [Eq. (3)] is the difference in energy between that of the strained lattice and the unstrained lattice. The equilibrium or unstrained lattice volume is V_0.

C_{ij} (in GPa)	Zinc blende	Rocksalt	Cooperite	Face centered orthorhombic
C_{11}	210	355	unstable	570
C_{22}	C_{11}	C_{11}	C_{11}	254
C_{33}	C_{11}	C_{11}	unstable	258
C_{44}	14	36	unstable	unstable
C_{55}	C_{44}	C_{44}	C_{44}	98
C_{66}	C_{44}	C_{44}	unstable	98
C_{12}	241	248	unstable	240
C_{13}	C_{12}	C_{12}	unstable	240
C_{23}	C_{12}	C_{12}	C_{13}	194

TABLE IV. All the independent elastic constants (in GPa) of PtN in different forms calculated using LDA. Symmetry dictates $C_{ij} = C_{ji}$ and all unlisted $C_{ij} = 0$. An unstable elastic constant in the table represents the case when the applied strain to the unit cell leads to a linear combination of C_{ij}'s to be negative. Elastic constants represented by C_{ij} instead of a numerical value imply that, that elastic constant is not an independent one, e.g., the value of elastic constant C_{22} of rock salt is equal to that of C_{11} already calculated to be 248 GPa. Notice that the condition $(C_{11} - C_{12}) > 0$ from Eq. (4) is not satisfied for zinc blende structure making it unstable.

Lattice Structure	Present work				Ref. [9]		Ref. [8]
	LDA		GGA		LDA	GGA	GGA
	VASP	WIEN2K	VASP	WIEN2K	WIEN2K	WIEN2K	WIEN2K
zb-PtN							
Bulk modulus (GPa)	230	235	192	178	244	194	371
Lattice constant (nm)	0.4699	0.4683	0.4794	0.4781	0.4692	0.4780	0.4804
E_{f-r-t} (eV)	0.42						
rs-PtN							
Bulk modulus (GPa)	284	298	226	233	-	-	431
Lattice constant (nm)	0.4407	0.4397	0.4504	0.4496	-	-	0.4518
E_{f-r-t} (eV)	0.75						
fco-PtN							
Bulk modulus (GPa)	270						
Lattice Constants nm)	a = 0.3972						
	b = 0.3977						
	c = 0.6022						
E_{f-r-t} (eV)	0.17						

co-PtN							
Bulk modulus (GPa)	-						
Lattice Constants (nm)	a = 0.3323						
	b = a						
	c = 0.4579						
E_{f-r-t} (eV)	0						

Table V. Bulk moduli (B) and lattice constants (a, b, c) of different phases of PtN obtained within the local density approximation (LDA) and the generalized gradient approximation (GGA). Two different *ab initio* methods were used in our work for zb-PtN and rs-PtN: (i) VASP [15,13,14,15], which uses a pseudopotential approach with plane wave basis and (ii) WIEN2K[35], which is an all electron FLAPW technique. Values from Ref. [8] and [9] are also computed using WIEN2K. The comparison shows that the bulk moduli calculated in the present work (VASP and WIEN2K) are in good agreement with Ref. [9] but differ by approximately 50% from those in Ref. [8]**.** [38] E_{f-r-t} is the **f**ormation energy per PtN formula unit with **r**espect to the **t**etragonal structure. Bulk modulus for tetragonal PtN is not reported as the involved elastic constants were found to be negative and unstable.

FIGURES

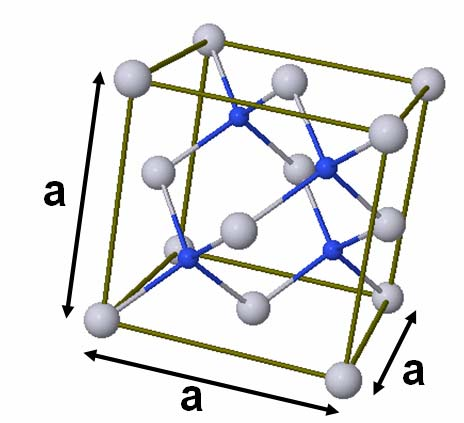

FIG. 1. Zinc blende structure of PtN. Larger (smaller) atoms are Pt (N). Only nearest neighbor bonds are shown. The lattice constant, a is given in Table V.

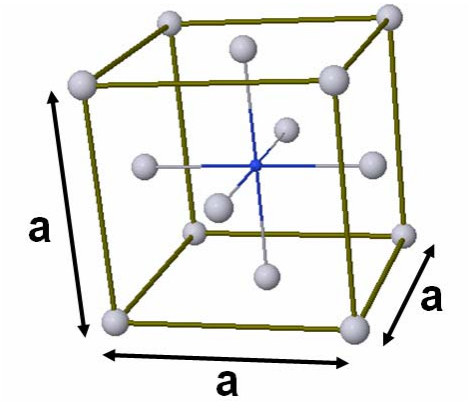

FIG. 2. Rock salt structure of PtN. Larger (smaller) atom is Pt (N). Only nearest neighbor bonds are shown. The N atoms at the center of each edge of the cube are not shown for clarity. The lattice constant, a is given in Table V.

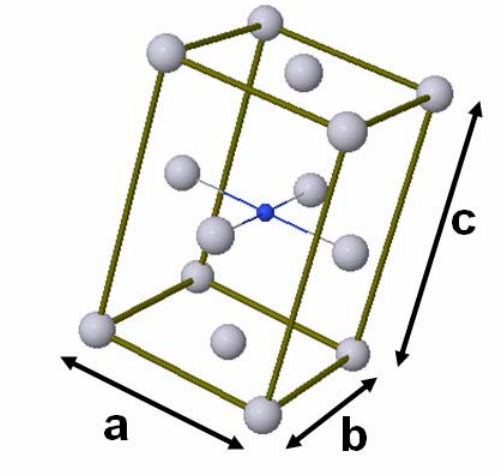

FIG. 3. Face centered orthorhombic structure of PtN. Larger (smaller) atom is Pt (N). Only nearest neighbor bonds are shown. The N atoms at the center of each edge of the cube are not shown for clarity. The lattice constants a, b and c are given in Table V.

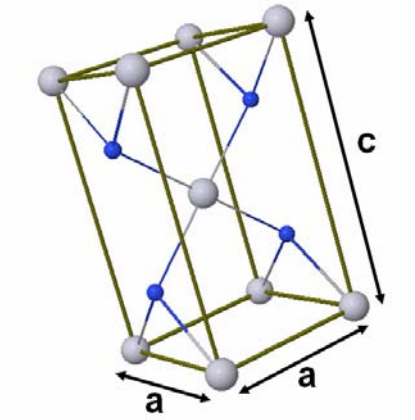

FIG. 4. Tetragonal structure of PtN. Larger (smaller) atom is Pt (N). Only nearest neighbor bonds are shown. The lattice constants a, c are given in Table V.

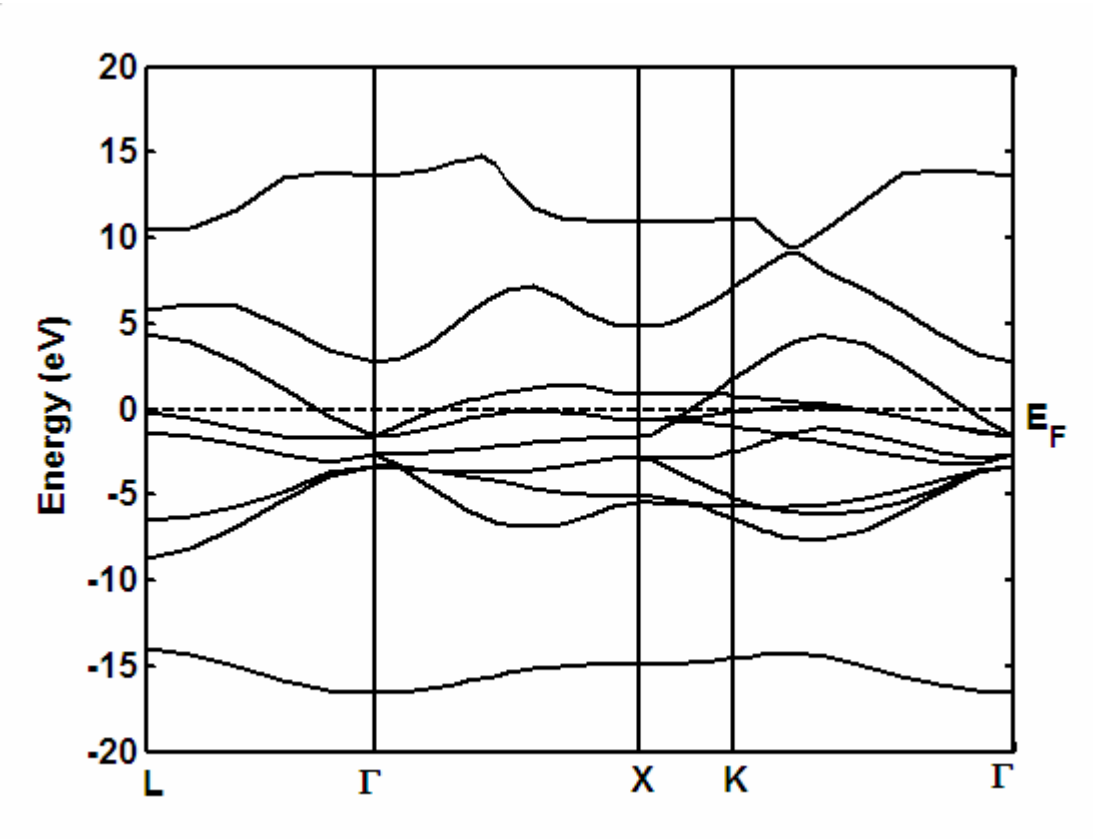

FIG. 5. Band structure of stable rocksalt structure of PtN along high symmetry points calculated using local density approximation (LDA) with Fermi energy level $\mathbf{E_F}$ taken at 0 eV as shown by the dotted line. The self consistent calculations were performed using ultra soft pseudopotentials with the theoretical lattice constant a given in Table V. The symmetry points considered in lattice coordinates are L $\left(\frac{1}{2},\frac{1}{2},\frac{1}{2}\right)$, X (0, 1, 0)[37], K$\left(\frac{3}{4},\frac{3}{4},0\right)$ and Γ (0, 0, 0).

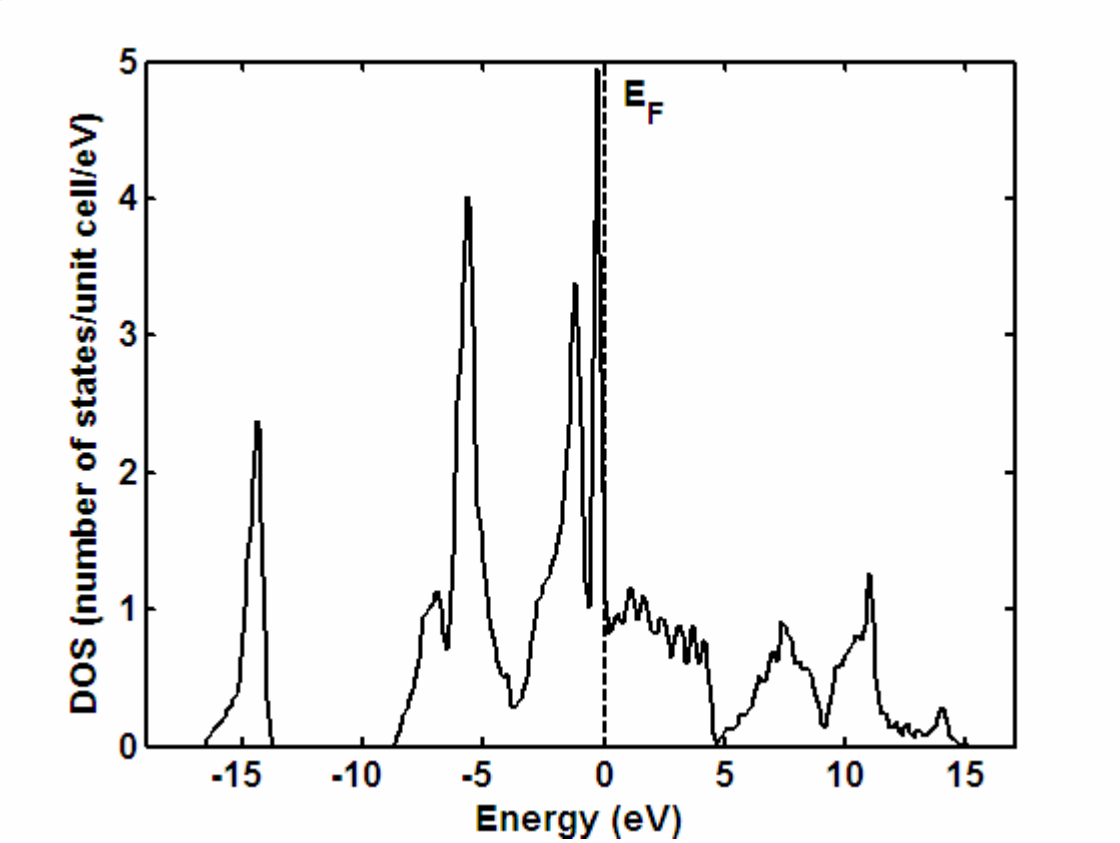

FIG. 6. Density of states (DOS) of stable rocksalt structure of PtN from local density approximation (LDA) calculations with $\mathbf{E}_F$, the Fermi energy level taken at 0 eV as shown by the dotted line. These calculations have been performed at the equilibrium theoretical lattice constant a given in Table V.

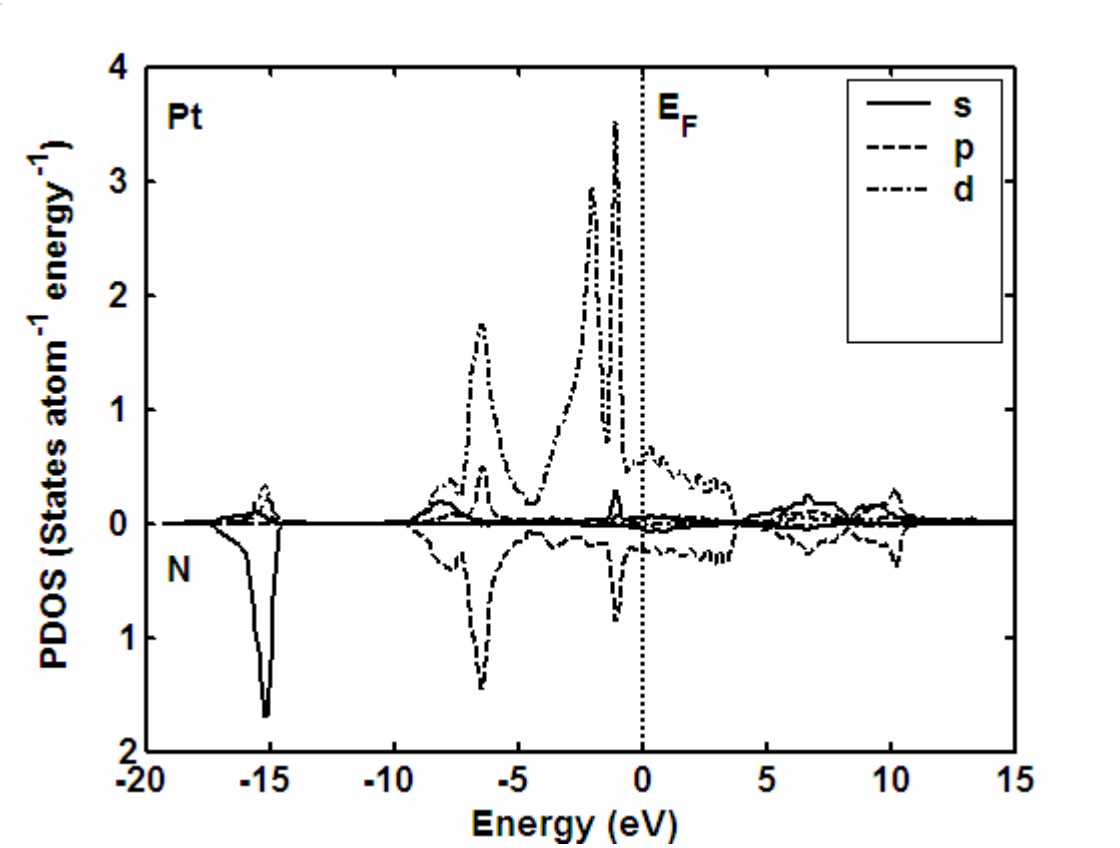

FIG. 7. s, p, and d projected density of states (PDOS) in the Pt and N spheres for stable rock salt phase of PtN with $\mathbf{E}_F$, the Fermi energy level taken at 0 eV as shown by the dotted line.